7856 *Biochemistry* **2009,** *48,* 7856–7866
DOI: 10.1021/bi901067b

BIOCHEMISTRY
including biophysical chemistry & molecular biology
*Article*

# Evidence that D1-His332 in Photosystem II from *Thermosynechococcus elongatus* Interacts with the $S_3$-State and not with the $S_2$-State[†]

Miwa Sugiura,*[,¶,||] Fabrice Rappaport,[§] Warwick Hillier,[‡] Pierre Dorlet,[⊥] Yohei Ohno,[||] Hidenori Hayashi,[¶,||] and Alain Boussac[⊥]

[¶]*Cell-Free Science and Technology Research Center, Ehime University, Bunkyo-cho, Matsuyama Ehime, 790-8577, Japan,* [||]*Department of Chemistry. Faculty of Science, Ehime University, Bunkyo-cho, Matsuyama Ehime, 790-8577, Japan,* [§]*Institut de Biologie Physico-Chimique, UMR 7141 CNRS-UPMC. 13 rue P et M Curie, 75005 Paris, France,* [‡]*Research School of Biology, The Australian National University, Canberra, ACT 0200, Australia, and* [⊥]*iBiTec-S, URA CNRS 2096, CEA Saclay, 91191 Gif sur Yvette, France*

*Received June 24, 2009; Revised Manuscript Received July 22, 2009*

ABSTRACT: Oxygen evolution by Photosystem II (PSII) is catalyzed by a $Mn_4Ca$ cluster. Thus far, from the crystallographic three-dimensional (3D) structures, seven amino acid residues have been identified as possible ligands of the $Mn_4Ca$ cluster. Among them, there is only one histidine, His332, which belongs to the D1 polypeptide. The relationships of the D1-His332 amino acid with kinetics and thermodynamic properties of the $Mn_4Ca$ cluster in the $S_2$- and $S_3$-states of the catalytic cycle were investigated in purified PSII from *Thermosynechococcus elongatus*. This was done by examining site-directed D1-His332Gln and D1-His332Ser mutants by a variety of spectroscopic techniques such as time-resolved UV−visible absorption change spectroscopy, cw- and pulse-EPR, thermoluminescence, and measurement of substrate water exchange. Both mutants grew photo-autotrophically and active PSII could be purified. On the basis of the parameters assessed in this work, the D1-His332(Gln, Ser) mutations had no effect in the $S_2$-state. Electron spin−echo envelope modulation (ESEEM) spectroscopy also showed that possible interactions between the nuclear spin of the nitrogen(s) of D1-His332 with the electronic spin $S = 1/2$ of the $Mn_4Ca$ cluster in the $S_2$-state were not detectable and that the D1-His332Ser mutation did not affect the detected hyperfine couplings. In contrast, the following changes were observed in the $S_3$-state of the D1-His332 mutants: (1) The redox potential of the $S_3/S_2$ couple was slightly increased by ≤20 meV, (2) The $S_3$-EPR spectrum was slightly modified, (3) The D1-His332Gln mutation resulted in a ∼3 fold decrease of the slow (tightly bound) exchange rate and a ∼2 fold increase of the fast exchange rate of the water substrate molecules. All these results suggest that the D1-His332 would be more involved in $S_3$ than in $S_2$. This could be one element of the conformational changes put forward in the $S_2$ to $S_3$ transition.

Light-driven water oxidation by the Photosystem II (PSII)[1] enzyme is responsible for the $O_2$ on Earth and is at the origin of the production of most of the biomass. Refined three-dimensional (3D) X-ray structures from 3.5 Å to 2.9 Å resolution have been obtained using PSII isolated from the thermophilic cyanobacterium *Thermosynechococcus elongatus* (*1*−*3*). PSII is made up of 20 membrane protein subunits, 35 chlorophyll molecules, 2 pheophytin molecules at least 12 carotenoid molecules, ≥ 25 lipids, 2 hemes, 1 nonheme iron, 2(+1) quinones, 4 Mn ions, 1 $Ca^{2+}$ ion, and at least 1 $Cl^-$ ion (*1*−*5*).

Absorption of a photon by a chlorophyll is followed by the formation of a radical pair in which the pheophytin molecule, $Pheo_{D1}$, is reduced and the accessory chlorophyll molecule, $Chl_{D1}$, is oxidized (*6*−*8*). The cation is then quickly transferred and stabilized on $P_{680}$, a weakly coupled chlorophyll dimer; see, for example, refs *9* and *10* for energetic considerations. The pheophytin anion transfers its unpaired electron to a quinone, $Q_A$, which in turn reduces a second quinone, $Q_B$. $P_{680}^{\bullet+}$ oxidizes a tyrosine residue of the D1 polypeptide, $Tyr_Z$, which in turn oxidizes the $Mn_4Ca$-cluster.

The $Mn_4Ca$-cluster acts as an oxidizing-equivalent accumulating device as well as the active site for water oxidation. During the enzyme cycle, the catalytic site goes through five sequential redox states, denoted $S_n$ where $n$ varies from 0 to 4 upon the absorption of four photons (*11*). Upon formation of the $S_4$ state two molecules of water are rapidly oxidized, the $S_0$-state is regenerated and $O_2$ is released.

The mechanism by which water is oxidized and $O_2$ is produced is still largely unknown, for example, refs *12*−*19*. First, uncertainties still remain as to the structure of the native $Mn_4Ca$ cluster owing to the reduction by the X-ray beam of the native high

[†]This study was supported in part by the JSPS and CNRS under the Japan-France Research Cooperative Program, by the EU/Energy project SOLAR-H2 (contract no. 212508), and by Grant-in-Aid for Young Scientists (B) from the Ministry of Education, Science, Sports, Culture and Technology (18770116 for M.S.).

*Corresponding author: E-mail: msugiura@chem.sci.ehime-u.ac.jp. Phone/Fax: 81 89 927 9616.

[1]Abbreviations: PSII, photosystem II; WT*, *T. elongatus* strain with a His-tag on the C terminus at CP43 and in which the *psbA1* and *psbA2* genes are deleted. Chl, chlorophyll; CP43 and CP47, chlorophyll-binding proteins; $P_{680}$, primary electron donor; $Q_A$, primary quinone acceptor; $Q_B$, secondary quinone acceptor; Pheo, pheophytin; DCBQ, 2,6-dichloro-*p*-benzoquinone; PPBQ, phenyl-*p*-benzoquinone, EPR, electron paramagnetic resonance; ESEEM, electron spin echo envelop modulation; TL, thermoluminescence; MES, 2-(*N*-morpholino) ethanesulfonic acid; $Me_2SO$; dimethyl sulfoxide; *Cm*, chloramphenicol; Sp, spectinomycin; Sm, streptomycin; βDM, beta dodecyl maltoside.

 Published on Web 07/22/2009 © 2009 American Chemical Society

valence $Mn_4Ca$ cluster back to the $Mn^{II}$ state (*20*, *21*). Second, the transition from $S_3TyrZ^{\bullet}$ to $S_0$ likely involves several reaction intermediates. Until now, these have largely escaped detection for various reasons among which (1) the reduction of $S_3TyrZ^{\bullet}$ is the limiting step for water oxidation in the native enzyme, and (2) experimental methods for trapping potential intermediate states are still lacking; see ref *22* for a recent elegant thermodynamic approach, the conclusions of which however have been recently challenged (*23*). For all these reasons, the mechanism of water oxidation still remains uncharacterized. As a consequence, the ligand environment of the $Mn_4Ca$-cluster and the role of the ligands in the overall mechanism still require being accurately characterized.

According to the structures (*1*−*3*), seven amino acids ligating the $Mn_4Ca$ cluster have been identified. Among these, six belong to the D1 protein (D1-Ala344, D1-Glu189, D1-His332, D1-Asp342, D1-Glu333, and D1-Asp170) and one belongs to the CP43 protein (CP43-Glu354). The role of these amino acids in maintaining a functional $Mn_4Ca$ cluster has been investigated by several groups before the 3D structures came out. This has been done by extensive site-directed mutagenesis in the mesophilic cyanobacterium *Synechocystis* 6803, reviewed in ref *15*. The confrontation of these studies to the 3D structure rises however an intriguing issue. Indeed, although the $S_2$ multiline EPR signal has been considered until now as being extremely sensitive to the environment of the $Mn_4Ca$ cluster, mutating most of the side-chains proposed to act as ligand to this cluster, the D1-Ala344-(Gly, Val, Asp, Asn) (*24*), D1-Glu189Gln (*25*, *26*), D1-Asp342Asn (*27*), D1-Asp170His (*28*), and CP43-Glu354Gln (*29*), had hardly any effect on the $S_2$ multiline EPR signal within experimental accuracy. In the case of D1-His337, an amino acid residue in the second coordination sphere, no spectroscopic studies have yet been reported on any D1-His337 mutant (*15*). For the D1-His332Glu mutant, the EPR characteristics were similar to those of a Ca-depleted sample; that is, the $S_2$ multiline signal was modified and the electron transfer was blocked after $S_2TyrZ^{\bullet}$ formation (*30*, *31*). Nevertheless, the low quantum yield for the formation of $S_2$ as well as the lack of the unusual stable $S_2$ state observed in $Ca^{2+}$-depleted PSII with these EPR characteristics were taken as arguments by the authors (*30*) against the release of $Ca^{2+}$ in the D1-His332Glu mutant.

In addition to the lack of modification of the $S_2$ multiline EPR signal several mutations are without any influence on the $S_n$-state cycle, at least in a fraction of the centers, such as D1-Glu189(Lys, Arg, Gln) (*25*, *26*), D1-Asp342Asn (*27*), D1-Asp170His (*28*). For D1-Ala344, D1-Glu189, D1-Asp342, D1-Glu333, and D1-Asp170, in most cases, the reported decrease in the activity of the mutants followed a decrease in the fraction of manganese containing PSII (*24*−*31*) suggesting, as already proposed for D1-Asp170His (*28*), that these amino acids are more essential to the assembly and/or the repair of PSII than to the oxygen evolution mechanism per se. There are four exceptions for which mutations strongly affect the electron transfer at the donor side. Surprisingly, these are (i) CP43-Arg357 (*32*), D1-Asp61 (*33*, *34*), and D1-His337 (*15*) which all belong to the second coordination sphere of the $Mn_4Ca$ cluster according to the 3D structures and (ii) the mutants at the D1-His332 position (*15*), as discussed above. For the latter, in *Synechocystis* 6803, any of the D1-His332 mutants which have been studied were photoautotrophic and only the D1-His332(Gln, Ser) mutants evolved oxygen in whole cells at 10−15% the rate of wild-type cells (*15*, *35*).

Since PSII isolated from *T. elongatus* is expected to be more robust than that purified from *Synechocystis* 6803, we have performed a study of D1-His332Gln and D1-His332Ser mutants in this thermophilic cyanobacterium with the hope that a high proportion of $O_2$ evolving PSII centers could be purified. This was indeed the case and we report here a characterization of these two mutants by a variety of spectroscopic techniques such as time-resolved UV−visible absorption change spectroscopy, cw- and pulse-EPR, Thermoluminescence and measurement of substrate water exchange. We found some evidence that the D1-His332(Gln, Ser) mutations affect some properties of the $S_3$-state.

## EXPERIMENTAL PROCEDURES

*Construction of the D1-His332Gln and D1-His332Ser Mutants*. Site-directed D1-His332Gln and D1-His332Ser mutations were constructed in the *psbA*$_3$ gene of the thermophilic cyanobacterium *Thermosynechococcus elongatus*. For creating mutations, the plasmid vector pUC19 inserting the *psbA*$_3$ gene (including 790 bp upstream and 870 bp downstream the *psbA*$_3$ open reading frame) and spectinomycin (Sp) and streptomycin (Sm) resistance gene cassette just after the stop codon of *psbA*$_3$ (*36*) was used. The mutations D1-His332Gln and D1-His332Ser were done by using a Quick-Change XL Site-Directed Mutagenesis kit (Stratagene). When making mutations, *Aat* II and *Bsp*H I recognition sites were created in D1-His332Gln and D1-His332Ser, respectively, around position of His as previously described (*36*, *37*, *39*). The DNA sequences are for D1-His-332Ser: ...ATGGAAG*TCATGA*GCGAGCGCAAT... and for D1-His332Gln: ...ATG*GACGTC*ATGCAGGAGCGCAAT... Characters that are in italic are the restriction enzyme recognition sites and characters that are underlined are the D1−332 position. The plasmids bearing mutations were transformed by electroporation into *T. elongatus* WT* cells. WT* was the host strain in which both the *psbA*$_1$ and *psbA*$_2$ genes were deleted (*36*) and which contains a $His_6$-tag fused to the C-terminus of CP43 (*38*). Single colonies were selected on DTN agar plate containing 12.5 $\mu$g of Sp·mL$^{-1}$, 5 $\mu$g of Sm·mL$^{-1}$, 20 $\mu$g of Km·mL$^{-1}$, and 2.5 $\mu$g of Cm·mL$^{-1}$. Segregation of all the *psbA*$_3$ copies in genome of the deletion mutant was confirmed by digestion of *psbA*$_3$ with *Aat* II and *Bsp*H I in D1-His332Gln and D1-His332Ser, respectively, after PCR amplification of the mutated region as described in refs (*36*−*38*). The sequences of the genomic DNA in the transformants which were used for this work, after complete segregation of the cells, were confirmed by using a CEQ2000 DNA Analysis System (Beckman).

*Purification of Thylakoids and PSII Core Complexes*. The transformed cells (and fully segregated) were grown in 1 L cultures of DTN in 3-L Erlenmeyer flasks in a rotary shaker with a $CO_2$-enriched atmosphere at 45 °C under continuous light in the presence of the corresponding antibiotics (see above). Thylakoids and PSII core complexes were prepared essentially as described earlier (*36*, *37*, *39*) with the following modifications. Glycerol was avoided from the elution step to the end of the purification. Indeed, glycerol was found to prevent the full detection of the $S_3$ EPR signal (*40*). The medium used to elute the PSII core complexes bound to the $Ni^{2+}$ resin contained 1 M betaine, 200 mM L-histidine, 100 mM NaCl, 15 mM $CaCl_2$, 15 mM $MgCl_2$, 40 mM Mes, 0.06% $\beta$DM, pH 6.5. After elution, PSII were washed and concentrated by using Amicon Ultra-15 concentrator devices (Millipore) with a 100 kDa cutoff. The washing medium and the final resuspending medium were 1 M betaine, 15 mM $CaCl_2$, 15 mM $MgCl_2$, 40 mM Mes, pH 6.5

(adjusted with NaOH). Routinely, the total amount of Chl before the breaking of the cells was ≈150−200 mg, and the yield after PSII purification in terms of Chl amounts was ≈3−5%. PSII were stored in liquid nitrogen at a concentration of about 2 mg of Chl·mL$^{-1}$. Betaine was used at a concentration of 1 M which has been shown to fully protect the $O_2$ activity in modified PSII and mutants in *T. elongatus* (*36*, *37*, *39*−*41*).

*Oxygen Evolution under Continuous Light*. Oxygen evolution of PSII under continuous light was measured at 25 °C by polarography using a Clark-type oxygen electrode (Hansatech) with saturating white light at a Chl concentration of 5 $\mu$g of Chl·mL$^{-1}$ in the media described above. A total of 0.5 mM DCBQ (2,6-dichloro-*p*-benzoquinone, dissolved in dimethyl sulfoxide) was added as an electron acceptor. The betaine, DCBQ, and $Q_B$ react in the minutes time range in the presence of $O_2$ (not shown). For that reason, measurement of PSII activity was done less than 1 min after the addition of DCBQ.

*Time Resolved UV*−*visible Absorption Change Spectroscopy*. Absorption changes were measured with a lab-built spectrophotometer (*42*) where the absorption changes are sampled at discrete times by short flashes. These flashes were provided by a neodymium:yttrium aluminum garnet (Nd:YAG) pumped (355 nm) optical parametric oscillator, which produces monochromatic flashes (1 nm full-width at half-maximum) with a duration of 6 ns. Excitation was provided by a dye laser (685 nm, 1 mJ) pumped by the second harmonic of a Nd:YAG laser. PSII was used at 25 $\mu$g of Chl·mL$^{-1}$ in 1 M betaine, 15 mM $CaCl_2$, 15 mM $MgCl_2$, and 40 mM MES (pH 6.5). PSII were dark-adapted for 1 h at room temperature before the additions of either 0.1 mM phenyl-*p*-benzoquinone (PPBQ, dissolved in $Me_2SO$) or DCMU (dissolved in ethanol).

*Thermoluminescence Measurements*. PSII core complexes were suspended in 1 M betaine, 15 mM $CaCl_2$, 15 mM $MgCl_2$, and 40 mM MES (pH 6.5), and thermoluminescence (TL) glow curves were measured with a lab-built apparatus (*43*). The Chl concentration was 0.2 $\mu$g of Chl·mL$^{-1}$. PSII were then dark-adapted for 1 h. The samples were illuminated at 5 °C by using a saturating xenon flash (SL-230S; Sugawara, Japan) and then rapidly chilled to 77 K with liquid $N_2$. The frozen samples were then heated at a constant rate of 40 °C·min$^{-1}$ and TL emission was detected with a photomultiplier (Hamamatsu, R943−02).

*EPR Spectroscopy*. cw-EPR spectra were recorded using a standard ER 4102 (Bruker) X-band resonator with a Bruker Elexsys 500 X-band spectrometer equipped with an Oxford Instruments cryostat (ESR 900). Flash illumination at room temperature was provided by a Nd:YAG laser (532 nm, 550 mJ, 8 ns Spectra Physics GCR-230-10). Pulsed EPR experiments were performed with a Bruker ESP580 spectrometer equipped with an Oxford Instruments cryostat. Field-swept and ESEEM spectra were recorded using a 3-pulse sequence $\pi/2-\tau-\pi/2-T-\pi/2-$ echo. The duration of the $\pi/2$ pulses was 16 ns. For the ESEEM, 800 points were recorded and T was incremented by 8 ns steps from its initial value equal to 60 ns. Fourier transform of the time domain data was done after: (1) subtraction of a background double exponential function, (2) zero-filling to 1024 points, (3) dead-time reconstruction by simulating peaks in the frequency domain followed by a back Fourier transform to fill the missing data in the dead time, and (4) Fourier transform of the full data (experimental + reconstructed dead time).

PSII samples at 1.1 mg of Chl·mL$^{-1}$ for cw-EPR and ≈ 4 mg of Chl·mL$^{-1}$ for pulse-EPR were loaded in the dark into quartz EPR tubes and further dark-adapted for 1 h at room temperature. Then, the samples for cw-EPR were synchronized in the $S_1$ state with one preflash (*44*). After another dark period of 1 h at room temperature, 0.5 mM PPBQ was added (the final concentration of dimethyl sulfoxide was ≈2%). Then, the samples were frozen in the dark to 198 K and then transferred to 77 K. Prior to the measurements the samples were degassed at 198 K as was already described (*39*).

Analysis of the data was done by using Excel (Microsoft), Mathcad 14 (Parametric Technology Corporation), and Origin 7.5 (OriginLab Corporation).

*Mass Spectrometric Measurements*. Frozen PSII core samples were thawed and diluted at 0.125 $\mu$mol of Chl·mL$^{-1}$ in the assay buffer containing 40 mM MES (pH 6.5), 15 mM $MgCl_2$, 15 mM $CaCl_2$, 10% glycerol, and 1.2 M betaine with 0.5 mM $K_3Fe(CN)_6$ serving as an electron acceptor. To circumvent prolonged dark adaptation/preflash cycles associated with the S-state lifetimes (*45*, *46*), the samples were loaded under complete darkness with IR goggles. The rapid mixing sample chamber interfaced to the mass spectrometer has been described earlier (*47*−*49*), and was temperature controlled to 10 °C. Experiments were performed using purified PSII preset into the $S_3$ state and injection (mixing rate $k_{inj}$ = 200 s$^{-1}$) of a 25 $\mu$L addition of 95% $H_2{}^{18}O$ to obtain the final $^{18}O$ enrichment of 12.0 ± 0.5%. The timing sequence and analysis are given in ref *49*. Analysis of the biphasic plots of $m/z$ = 34 exchange were fit to the sum of two exponential functions revealing a fast phase $k_2$ and slow phase $k_1$ of $H_2{}^{18}O$ exchange.

$$Y_C = 0.57(1-\exp(-k_2t)) + 0.43(1-\exp(k_1t)) \quad (1)$$

Analysis of the $m/z$ = 36 exchange was to a single exponential function arising from the rate determining slow exchange $k_1$ of $H_2{}^{18}O$ exchange.

$$Y_C = 1-\exp(k_1t) \quad (2)$$

The two data sets were globally fit with eqs 1 and 2 to derive one set of $k_1$ parameters.

## RESULTS

To study the effects of the D1-His332 mutations on water splitting, we conducted various spectroscopic studies on the $Mn_4Ca$ cluster in PSII. First, we examined $O_2$ evolution under steady-state illumination. The activity of purified WT* PSII was routinely determined as 4500−6000 $\mu$mol of $O_2$/mg of Chl·h$^{-1}$, whereas activity in the mutants was somewhat lower at 3800−4500 $\mu$mol of $O_2$/mg of Chl·h$^{-1}$. The $O_2$ activity of *T. elongatus* after D1-His332(Gln,Ser) mutations is much greater than in the case of similar mutations in *Synechocystis* PCC 6803 since in these mutant strains the photoautotrophic growth was 10−15% of wild type cells (*35*). In the *T. elongatus*, the activity in purified PSII was decreased by ∼20% when compared to WT* PSII.

To gain further insight into integrity and potential turnover limitations of the $Mn_4Ca$ cluster transient absorption spectroscopy was performed at 292 nm to follow the oxidation changes of the Mn ions. The measurements were done at 19 °C. Figure 1 shows the $S_n$-state cycle probed by the amplitude of the flash-induced absorption changes in the WT*, the D1-His332Gln mutant and the D1-His332Ser mutant. Absorption measurements at 292 nm were recorded in the hundred of millisecond time range; that is, after the reduction of $Tyr_Z^{\bullet}$ by the $Mn_4Ca$ cluster was complete. This wavelength corresponds to an isosbestic point for $PPBQ^-$/PPBQ (not shown), the added electron acceptor, and is in a spectral region where the absorption of the $Mn_4Ca$ cluster

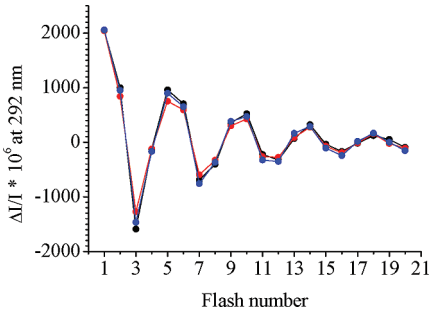


FIGURE 1: Sequence of the amplitude of the absorption changes at 292 nm during a series of saturating flashes spaced 400 ms apart and given on WT*-PSII (black symbols), D1-His332Gln PSII (red symbols), and D1-His332Ser PSII (blue symbols). The samples at 25 $\mu$g of Chl/mL were dark-adapted for 1 h at room temperature before the addition of 100 $\mu$M PPBQ (dissolved in Me2SO). The measurements were done 100 ms after each flash.

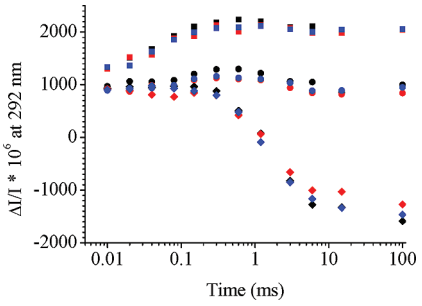


FIGURE 2: Kinetics of the absorption changes at 292 nm after the first flash (squares), the second flash (circles), and the third flash (diamond) given to dark-adapted WT*-PSII (black), D1-His332Gln PSII (red), and D1-His332Ser PSII (blue). Other experimental conditions were similar to those in Figure 1.

depends on the S-states (*50*, *51*). The oscillating pattern with a period of four is clearly observed for all three types of PSII preparations in Figure 1. By using the formula developed by Lavorel (*52*) and the analysis developed by Lavergne (*51*), the three oscillating patterns shown in Figure 1 were fitted together as previously described (*46*). Each of the three different differential extinction coefficients, $\Delta\varepsilon_0$, $\Delta\varepsilon_1$, $\Delta\varepsilon_2$, corresponding to the $S_0$ to $S_1$, $S_1$ to $S_2$, and $S_2$ to $S_3$ transitions, respectively, were kept fixed for the three types of PSII and they were found equal to $400 \times 10^{-6}$, $1500 \times 10^{-6}$, and $1200 \times 10^{-6}$, respectively, in $\Delta I/I$ unit for the sample concentration (25 $\mu$g of Chl/mL) and path length (2.5 mm). In this experiment, a double hit parameter, 4−5%, was used to account for the small actinic effect of the measuring beam. The miss parameter was found to be close to 10% for the three samples. The $S_0/S_1$ ratio was allowed to vary for each type of sample. It was found to be 0/100 for the WT* PSII and 10/90 for the two mutants (Supporting Information).

The results in Figure 1 show that in purified PSII both the D1-His332Gln and D1-His332Ser mutations neither significantly alter the $S_n$-state cycle in terms of transition probability, nor increase the fraction of inactive PSII centers based on the absorption at 292 nm per unit of Chl concentration. Therefore, the slightly smaller $O_2$ evolution activity under continuous illumination in purified PSII does not reflect a lower proportion of active centers in the D1-His332Gln and D1-His332Ser mutants but rather a slight kinetic limitation.

Although the period four oscillation pattern was hardly affected by the mutations, we characterized the kinetics of electron transfer associated with each of the individual steps to gain further insights into the consequences of the mutations. For that we recorded the absorption changes at 292 nm over the microsecond to millisecond time-range after each flashes of a series given to dark-adapted PSII (Figure 2). Absorption changes at this wavelength reflect the $Mn_4Ca$-cluster valence change and the $Tyr_Z$ redox state change occurring in the $S_1Tyr_Z^\bullet$ to $S_2Tyr_Z$, $S_2Tyr_Z^\bullet$ to $S_3Tyr_Z$, $S_3Tyr_Z^\bullet$ to $S_0Tyr_Z$ and $S_0Tyr_Z^\bullet$ to $S_1Tyr_Z$ transitions (*46*, *50*, *51*). As shown in Figure 2, the transient absorption changes hardly differed between the three samples after the first, second, and third flash (and also in subsequent flashes, data not shown). Increasing the temperature up to 53 °C, a more physiological temperature for *T. elongatus*, reduced the miss parameter to ≈5% in both the WT* and mutant PSII (not shown). Time-resolved absorption changes measured at 53 °C and at 292 nm revealed no kinetic differences between the WT* and the D1-His332Gln and D1-His332Ser mutants (not shown).

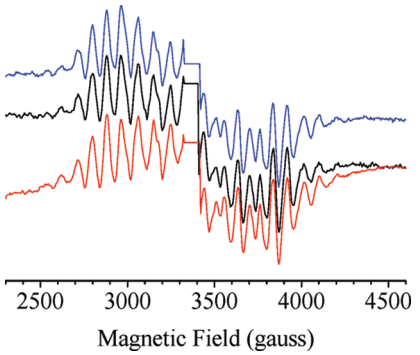


FIGURE 3: Light *minus* dark EPR spectra induced by one flash at room temperature in the presence of 1 mM PPBQ and recorded on WT*-PSII (black spectrum), D1-His332Gln PSII (red spectrum), and D1-His332Ser PSII (blue spectrum). Sample concentration was 1.1 mg of Chl/mL. A preflash was given to synchronize all the centers in $S_1$. Instrument settings: modulation amplitude, 25 gauss; microwave power, 20 mW; microwave frequency, 9.4 GHz; modulation frequency, 100 kHz; Temperature, 8.5 K. The central part of the spectra corresponding to the $Tyr_D^\bullet$ region was deleted.

As mentioned in the introduction, site-directed D1-His332Glu mutation in *Synechocystis* 6803 resulted in the complete inhibition of the $S_n$-state cycle after $S_2Tyr_Z^\bullet$ formation as well as in a modified multiline EPR signal in the $S_2$ state (*30*, *31*). The EPR multiline spectrum arising from the $S_2$ state is centered at $g \approx 2$ and spread over about 1800 G. It is made up of at least 18 lines, each separated by approximately 80 G, and arises from a spin 1/2 (ground) state, very likely from a magnetic Mn tetramer, $Mn^{IV}{}_3Mn^{III}$ (*53*−*56*). Since the parameters determining the rate of the $S_n \rightarrow S_{n+1}$ transitions are largely unknown, the possibility that the mutations affect the environment of the $Mn_4Ca$ cluster with little consequences on the rates remains. Because it probes the spin coupling between the Mn ions in the tetramer, EPR spectroscopy is well suited to characterize possible changes in the coordination sphere of the Mn ions. The results in Figure 3 show that in the D1-His332Gln and D1-His332Ser mutants both the amplitudes and shapes of the $S_2$-multiline signal recorded after one flash given at room temperature were indistinguishable from that in WT*-PSII.

The resolved hyperfine structure of the $S_2$ multiline EPR spectrum originates from the interaction between the electronic and the nuclear spins of the four Mn ions. To obtain information on the interactions between the electronic spin and the surrounding nuclei of the solvent and/or the protein matrix a technique allowing the resolution of the weak hyperfine interactions is required. ESEEM spectroscopy is suited for doing so, and

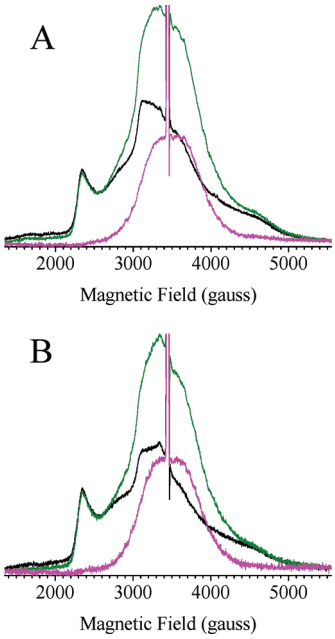


FIGURE 4: Field-swept echo spectra in WT* (A) and D1-His332Ser (B). The amplitude of the spectra was normalized to the same PSII concentration by using the $Tyr_D^{\bullet}$ signal as a reference. Spectra were recorded in the dark-adapted state (black spectra) and after illumination at 200 K (green spectra). The magenta spectra are the light *minus* dark spectra. The echo resulted from a three-pulse sequence $\pi/2-\tau-\pi/2-T-\pi/2-$echo. The spectra shown are the sum of spectra recorded for $T = 60$ ns and $\tau$ values equal to 136, 168, 200, and 232 ns. Temperature, 4.2 K; microwave frequency, 9.7 GHz. Shot repetition time = 8 ms. The central part of the spectra corresponding to the $Tyr_D^{\bullet}$ region was deleted.

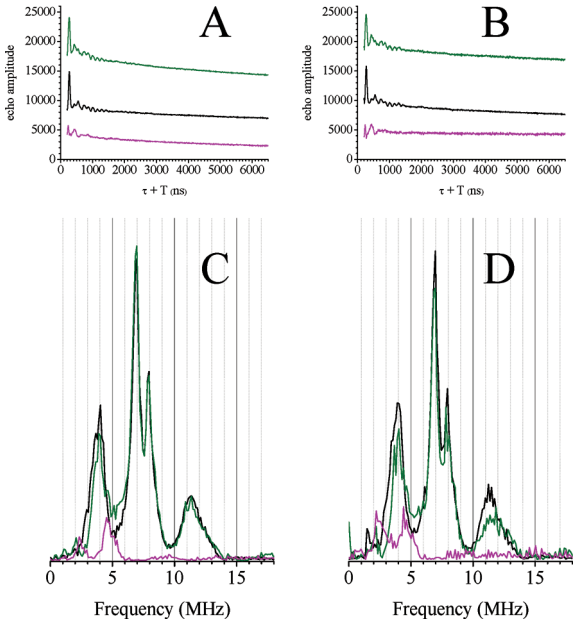


FIGURE 5: ESEEM spectra in WT* PSII and D1-His332Ser PSII. Time domain spectra (A and B) and frequency domain spectra (C and D) recorded in WT* PSII (A and C) and D1-His332Ser PSII (B and D). The black traces were recorded in the dark-adapted samples, the green traces after 200 K illumination and the magenta traces are the light *minus* dark ESEEM in panels A and B, and the Fourier transform of the light *minus* dark ESEEM in panels C and D. In panels A and B, the light *minus* dark ESEEM (magenta) were down shifted by 5000 arbitrary units for clarity. Magnetic field = 3540 gauss; temperature, 4.2 K; microwave frequency, 9.7 GHz. Shot repetition time = 8 ms.

the results of such an approach are shown in Figure 4 for the WT* PSII and the D1-His332Ser mutant. The D1-His332Gln mutant was not used here since this substitution maintains a nitrogen in the possibly interacting amino acid side-chain.

Figure 4 shows the field-swept spectra in WT* PSII (panel A) and D1-His332Ser PSII (panel B). Spectra were recorded in the dark-adapted samples (black spectra) and after illumination at 200 K (green spectra), that is, in the $S_2$-state. The magenta spectra show the difference between the spectra obtained after illumination and in the dark. The spectra recorded in the dark-adapted samples, that is, in the $S_1$-state, arise from the fully oxidized Cyt$c_{550}$ and possibly from a low amount of oxidized Cyt$b_{559}$ (*57*, *58*). The light-induced field-swept spectra correspond to the $S_2$-multiline signal. As for the cw-EPR experiment, Figure 4 shows that the $S_2$ signal induced by 200 K illumination had a similar amplitude in the WT* PSII and D1-His332Ser PSII samples.

To disentangle the various species which may contribute to the ESEEM spectra, these were recorded in $S_1$ and $S_2$ at nine magnetic field values from 2340 to 3940 gauss by 200 gauss steps and with $\tau$ values equal to 136, 168, 200, and 232 ns. At 2340 gauss, only the cytochrome(s) contribute(s) to the spectra. At this magnetic field value, the light *minus* dark spectrum was featureless, indicating that upon illumination at 200 K the cytochrome(s) do not undergo any redox changes and thus do not contribute to the light-induced changes in the ESEEM spectra.

Figure 5 shows the time domain (panels A and B) and the frequency domain (panels C and D) recorded in WT* PSII (panels A and C) and D1-His332Ser PSII (panels B and D). The black traces were recorded in the dark-adapted sample, the green traces after 200 K illumination. The magenta traces are the light *minus* dark ESEEM (panels A and B) and the Fourier transform of the light *minus* dark ESEEM (panels C and D). In panels A and B, the light *minus* dark ESEEM (magenta) were down shifted by 5000 arbitrary units for clarity.

The amplitude of the modulations arising from the multiline signal is rather weak when compared to the amplitude of the peaks at ≈4, 7, 8, and 11.5 MHz recorded in the $S_1$-state and which very likely arise from the tetrapyrrole nitrogen(s) of Cyt $c_{550}$. These frequencies are very similar to those arising from Cyt $b_{559}$ (*59*). Because of the $\tau$ value used here and the magnetic field value at which the data were recorded, the free proton frequency at 14−15 MHz was suppressed. Fortunately, the peaks in the Fourier transform of the light *minus* dark ESEEM spectra are different from those arising from the cytochromes which confirms that the light *minus* dark spectra are free from contributions from the cytochrome signals. Figure 5C shows that small peaks at around 2.5 and 4.5 MHz are found with the WT* PSII as observed previously in *Synechocystis* 6803 (*31*). In the D1-His332Ser mutant (Figure 5D), the spectra are identical to those in WT* in the limit of the signal-to-noise ratio. The very small difference in the relative amplitude of the peaks at 2.5 and 4.5 MHz in the mutant and the WT* sample is not significant. Similar results were obtained at the other magnetic field values and with the other $\tau$ values (not shown).

The thermodynamic properties of the $S_2$ state in the mutants were investigated by measuring the thermoluminescence arising from the $S_2Q_B^-$ charge recombination. Figure 6 shows no significant change in the peak temperature of the TL glow curves arising from the $S_2Q_B^-$ charge recombination in the D1-His332Gln mutant and only a down shift by 2 °C from 50 to 48 °C in the D1-His332Ser mutant when compared to that observed for the WT* PSII. This indicates that the Em of the

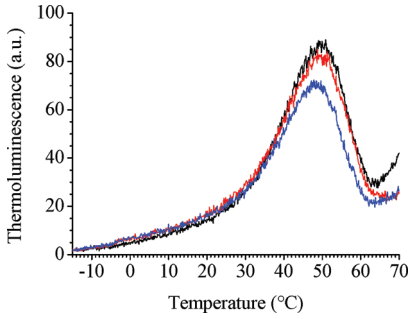


FIGURE 6: Thermoluminescence glow curves from $S_2Q_B^{\bullet -}$ charge recombination. TL glow curves were recorded after one flash in PSII from WT*-PSII (black trace), D1-His332Gln PSII (red trace), and D1-His332Ser PSII (blue trace).

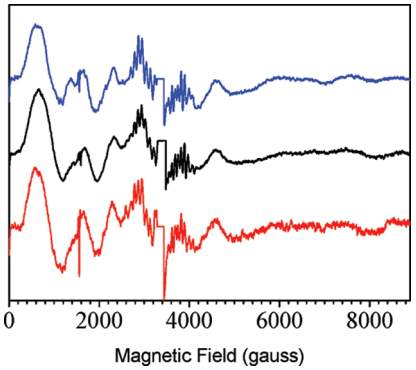


FIGURE 7: Light *minus* dark EPR spectra induced by two flashes at room temperature in the presence of 1 mM PPBQ and recorded on WT*-PSII (black spectrum), D1-His332Gln PSII (red spectrum), and D1-His332Ser PSII (blue spectrum). Sample concentration was 1.1 mg of Chl/mL. A preflash was given to synchronize all the centers in $S_1$. Instrument settings: modulation amplitude, 25 G; microwave power, 20 mW; microwave frequency, 9.4 GHz; modulation frequency, 100 kHz, temperature, 8.5 K. The $Tyr_D^{\bullet}$ spectral region at $g \approx 2$ was deleted. The multiline signal detected after two flashes originates from centers still in $S_2$ and this is due to the ≈ 10% misses mentioned in the text.

$S_2/S_1$ couple in the D1-His332 mutants is not significantly affected. Consistent with this the kinetics of $S_2Q_A^-$ charge recombination, as observed by measuring the decay of $Q_A^-$ at 320 nm, were similar in the WT* and mutant PSII (not shown).

All the data reported above indicate that in *T. elongatus* the D1-His332(Gln, Ser) mutations do no affect significantly the thermodynamic, kinetic, or structural properties of the $S_2$-state. Yet, the possibility remains about the other $S_n$-states and in particular the $S_3$ state the formation of which is associated with significant conformational changes (*60*−*64*).

To address this issue, we relied on the recently reported cw-EPR spectrum of the $S_3$ state in WT* PSII (*40*). This signal has been shown to originate from a spin $S = 3$ state. Figure 7 shows the $S_3$ EPR spectrum recorded in the D1-His332(Gln, Ser) mutants. The field positions of the resonances are roughly similar in the mutants and the WT*. Therefore, the zero field splitting parameters in the mutants PSII and the WT* PSII should be not significantly modified. Nevertheless, a close examination of the spectra revealed that the main feature at around 600 gauss is reproducibly down shifted by ≈150 gauss (Supporting Information).

The redox properties of the $S_3$-state were probed by TL experiment. Figure 8 shows the TL glow curves of the $S_3Q_B^-$ charge recombination. Although the peak temperature in the D1-His332Ser PSII is only down-shifted by 2 °C (as for $S_2Q_B^-$)

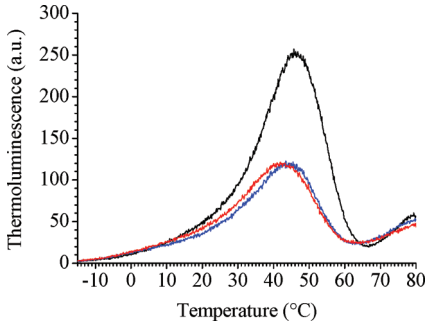


FIGURE 8: Thermoluminescence glow curves from $S_3Q_B^{\bullet -}$ charge recombination. TL glow curves were recorded after two flashes in PSII from WT*-PSII (black trace), D1-His332Gln PSII (red trace), and D1-His332Ser PSII (blue trace).

that in the D1-His332Gln PSII is down shifted by ≈4 °C from 46 to 42 °C. A qualitative estimate of the change of the Em of the $S_3/S_2$ couple at the origin of this 4 °C down shift can be obtained by comparing the shift in Tm observed here with those reported previously in the literature and associated with a known change in a free energy gap. For example, in *T. elongatus*, a point mutation in the vicinity of $Q_A$ has been found to induce a shift in Tm of 9 °C and a change in free energy of ≈60 meV (*65*). Therefore, the down shift of 4 °C could correspond to an increase of ≈27 meV of the Em of the $S_3/S_2$ couple in the mutants. Numerical simulations of TL glow curves indicated that the Tm depends linearly on the $\Delta H$ of the direct route with a slope of ≈0.4 °C/meV (*66*). Such a dependency would suggest an increase in the Em of the $S_3/S_2$ couple in the mutants of 10 meV. The analysis of both the kinetics of the charges recombination and TL glow curves in various PSII mutants in *Synechocystis* 6803 resulted in ≈0.2 °C/meV (*67*). Therefore, by averaging the data in these three previous works (*65*−*67*) the increase of the Em of the $S_3/S_2$ couple in the D1-His332(Gln,Ser) mutants can be estimated to be ≈20 meV.

Figure 8 shows that for the $S_3Q_B^-$ charge recombination the amplitude of the TL glow curve for WT* PSII was twice that of the D1-His332(Gln, Ser) mutants. This smaller amplitude of the TL glow curve in the mutants is in agreement with an increase in the Em of the $S_3/S_2$ couple in these mutants (*66*, *67*).

Alternatively, we followed the decay of the $S_3Q_B^-$ state by measuring the time-course of the $S_3$ EPR spectrum after two flashes (Figure 9). The samples were frozen at various times after the two flashes given at room temperature, and the amplitude of the signal at around 800 gauss was measured. Fitting the data with a single exponential decay and an offset to account for the proportion of centers in the $Q_B$ state (≈20%) yielded half times of ≈3.5 min in WT* PSII and ≈2.9 min in the mutants. Such a difference in the $t_{1/2}$ indicates an increase by ≈60 log(3.5/2.9) = 5 meV of the $S_3/S_2$ couple in the mutants. This is less than expected from the TL experiments. This difference may stem from the intrinsic complexity of the $S_3Q_B^-$ charge recombination which is a polyphasic process, the slow components of which could be more affected by the mutation than the fast phase. Indeed, one has to keep in mind that the TL experiments mainly probe the slower charge recombination processes as discussed previously (*68*). The number of data points in Figure 9 does not allow a reliable fit of the data with two exponentials leaving this possibility open.

It has been shown earlier that the binding properties of the two water molecules could be resolved in $S_3$ (*47*) and that these properties were strongly affected either by Ca/Sr exchange or by

some mutations in the $Mn_4Ca$ cluster environment (*16*, *29*, *33*, *48*, *49*). The results above suggest that the D1-His332(Ser, Gln) mutations in *T. elongatus* slightly affect the thermodynamic and structural properties of the $S_3$ state, and we thus studied water exchange to examine the consequences on substrate binding.

The results from the $^{18}O$ exchange measurements of the WT* and D1-His332Gln mutant PSII core samples are shown for the $S_3$ state in Figure 10 and in Table 1. The $m/z = 34$ data reveal biphasic kinetics and the $m/z = 36$ data are monophasic and have both been shown to be characteristic for the two substrate water sites that have been seen in all other PSII samples (*16*, *29*, *33*, *47*−*49*). The WT* material (black circles) and D1-His332Gln data (red circles) are presented in Figure 10 along with the fitted exchange kinetics (solid lines) according to eq 1 for $m/z = 34$ and eq 2 for $m/z = 36$ in Figure 10. The inset to the $m/z = 34$ data in Figure 10 shows a shorter time scale to better compare the fast phase. The exchange rates for WT* PSII were found to be $k_1 = 0.40 \pm 0.02\ s^{-1}$ and $k_2 = 18.9 \pm 1.0\ s^{-1}$ for the slow and fast phases, respectively. The D1-His332Gln mutation gave exchange rates of $k_1 = 0.15 \pm 0.01\ s^{-1}$ and $k_2 = 37 \pm 5\ s^{-1}$. The indication from these results is a measurable change in both substrate water binding sites. The D1-His332Gln mutation results in a ~3 fold decrease of the slow (tightly bound) exchange rate and a ~2 fold increase of the fast exchange rate. Thus, both sites appear to be perturbed by the D1-His332Gln mutation. The perturbation of both the slow and fast exchange substrate sites is one indication of a direct change in the substrate binding affinity resulting from the D1-His332Gln mutation.

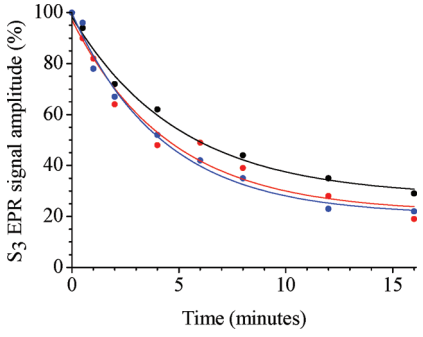


FIGURE 9: Decay at room temperature of the $S_3$-state in WT* PSII (black), D1-His332Gln PSII (red), and D1-His332Ser PSII (blue). The $S_3$-state was followed by recording the $S_3$ EPR spectrum shown in Figure 7 as a function of the time between the two flashes spaced 1 s apart and the freezing of the sample. A preflash protocol was used, but no PPBQ was added to keep $Q_B^-$ present at time $t = 0$. Instrument settings as in Figure 7.

## DISCUSSION

A number of amino acid residues have been implicated in the coordination of the $Mn_4Ca$ cluster where the oxidation of water is catalyzed and the O−O bond is templated. Thus far, seven amino acids have been identified as possible ligands in the 3D structure (*1*−*3*). This includes residue D1-His332 which is interesting as this is likely to be the only histidine coordination to the $Mn_4Ca$ complex. The histidine residue has interesting chemical properties associated with its p*K* and the interaction with the OEC is an important question to resolve. The relationships of the D1-His332 amino acid with kinetics and thermodynamic properties of the $Mn_4Ca$ cluster were investigated in PSII from *T. elongatus* by examining the D1-His332(Gln,Ser) mutants.

In analyzing these mutants, we found both mutants grew photoautotrophically and active PSII can be purified. Oxygen evolution activity in the D1-His332(Gln, Ser) mutants was found to be approximately 80% of that measured in WT* PSII. Yet, the same mutation constructed in *Synechocystis* PCC 6803 did not allow the authors (*15*, *35*) to purify active PSII centers. This difference suggests that the thermostability of *T. elongatus* offers an improved capacity for viability with mutation at this site. This may be the result of stronger ligation of the remaining metal ligands or it may offer an aspect of coordination compensation within the oxygen evolving complex.

Table 1: Rate Constants for $^{18}O$ Exchange in the $S_3$ State of PSII Core Complexes from WT* and a Mutant of *T. elongatus*

| sample | $k_1\ (s^{-1})$ | $k_2\ (s^{-1})$ |
|---|---|---|
| WT* | $0.40 \pm 0.02$ | $18.9 \pm 1.0$ |
| D1-His332Gln | $0.15 \pm 0.01$ | $37 \pm 5$ |

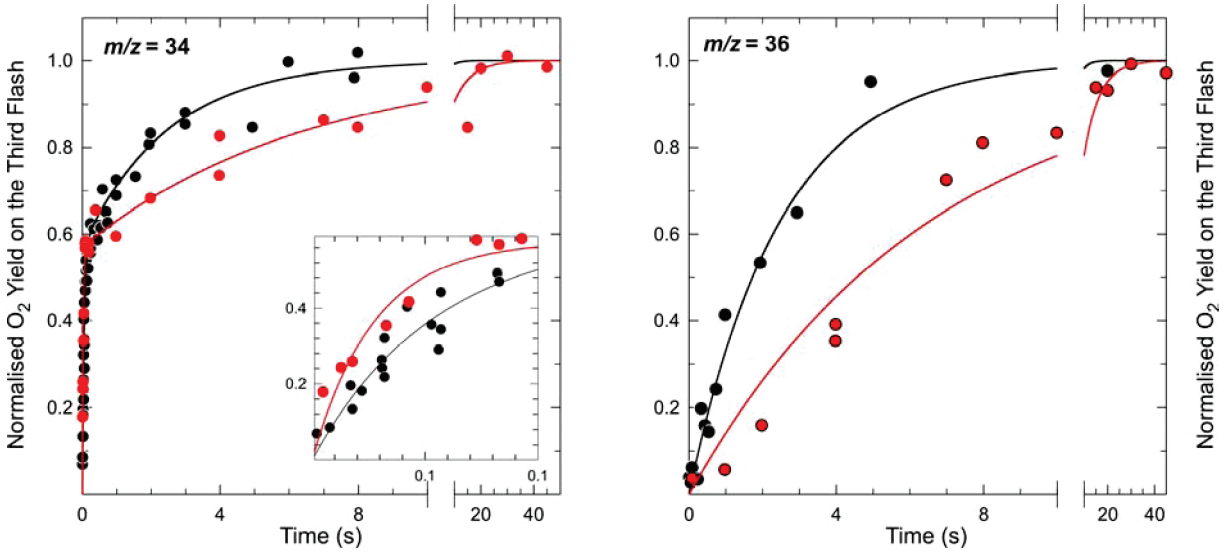


FIGURE 10: Water $^{18}O$ exchange measurements in the $S_3$ state of purified PSII from WT* and D1-His332Gln mutant. The WT* data are shown in black and the D1-His332Gln data are shown in red. The inset is a shorter time expanded to show the fast phase.

The analysis of the flash patterns (Figure 1) provides for a capacity to analyze functional centers and turnover efficiency. The flash dependence of the profile showed that the turnover efficiencies were not at all perturbed by the mutations. The absence of any major consequences of the two mutations on the turnover of the $S_n$-state cycle (Figure 1) under flashing conditions and the lack of significant changes in the kinetics of the $S_i \rightarrow S_{i+1}$ transition, and particularly in the kinetics of the $S_3$ to $S_0$ transition, suggest that the slight decrease in the $O_2$ evolution activity under continuous illumination likely results from the integration of several limited kinetics effects which escaped detection when studying separately the individual steps in the catalytic cycle. The slightly smaller $S_1/S_0$ ratio in the mutants upon dark adaptation could also reflect the small differences in electron transfer reactions and equilibria between the redox cofactors. In addition, we cannot totally exclude long-range effects of the mutations on the acceptor side.

On the basis of experiments reported here, it appears that the D1-His332(Gln, Ser) mutations have no effect in the $S_2$ state, at least for the parameters assessed in this work. This differs from the situation in *Synechocystis* 6803 in which the absence of His332 resulted in modified EPR and TL characteristics (*30*, *69*).

A pulse-EPR study performed in the $S_2$ state and aiming at determining whether the D1-His332 was a ligand of the $Mn_4Ca$ cluster (and performed before the publication of the 3D structures) (*31*) concluded that a histidyl nitrogen modulation observed near ≈5 MHz was substantially diminished in D1-His332Glu PSII. The peak at ≈5 MHz was shown to originate from the imidazole side chain of a histidine (*70*). Therefore, as proposed by the authors in ref *31*, since the multiline signal was altered in the D1-His332Glu mutant, the 4.5 MHz peak could originate from the nitrogen-nucleus of another histidine, possibly D1-His337 from the structures published after the work in ref *31*. In this model, the magnetic coupling between the nuclear spin of this nitrogen and the electronic spin of the $Mn_4Ca$ cluster would be modified by the same structural change as that at the origin of the $S_2$ multiline modification in the D1-His332Glu mutant. In *T. elongatus* in which the D1-His332Ser mutant does not exhibit a $S_2$ multiline modification it is shown here that the frequency peaks at around 2.5 and 4.5 MHz do not decrease. This means that (i) the peaks at 2.5 and 4.5 MHz observed in pulse-X-band EPR do not originate from the nitrogen(s) of the imidazole ring of D1-His332, (ii) the histidyl nitrogen(s) of D1-His332 were not detected by ESEEM performed at X-band, (iii) the mutation does not change the magnetic coupling between the multiline signal and this/these nitrogen(s), (iv) the 2.5 and 4.5 MHz could originate from the nitrogen(s) of the imidazole ring of D1-His337, (v) the results in *Synechocystis* 6803 likely originate from the structural changes at the origin of the $S_2$ multiline signal modifications which would be a kind of secondary effect which would remain to be explained.

With the exception of D1-His332 (see above) none of the six other potential ligands identified by 3D crystallography, that is, D1-Ala344 (*24*), D1-Glu189 (*25*, *26*), D1-Asp342 (*27*), D1-Asp170 (*28*), D1-Glu333 (*35*), and CP43-Glu354 (*29*), seem to be essential for the activity in *Synechocystis* 6803. One may speculate that they have other roles in the assembly, stability, and/or the repair of PSII rather than a direct role for oxygen evolution mechanism itself (see introduction). However, it is also possible that coordination is viable with these ligands and the mutations are rescued. From the present work, D1-H332 appears also not essential for the water oxidation mechanism.

In *Synechocystis* 6803, for the three mutants D1-Asp342Asn (*27*), D1-Asp170His (*28*), and D1-Glu189(Gln, Arg) (*25*), see however ref *26*, in which the FTIR spectra have been recorded in all the S-state transitions, none of these mutations induces significant spectral change. This was interpreted by a model in which the Mn ions ligated by these amino acids were not oxidized during the $S_n$-state cycle. It was, for example, proposed that the Mn ion oxidized in the $S_1$ to $S_2$ transition was that ligated by D1-Ala344 (*71*). Nevertheless, it is striking that such a sensitive method is blind for most of the mutants around the $Mn_4Ca$ cluster.

Similarly, the $S_2$ EPR multiline signal has been found to be not susceptible to the change of six of its ligands. This could suggest that this is the $Mn_4Ca$ cluster, provided it is correctly assembled, which structures the protein around it. It seems that the missing ligands in the 3D structure, possibly water molecules, are more important in maintaining the $Mn_4Ca$ structure, at least in the $S_2$ state, than thought until now. It is indeed difficult to explain why the $Ca^{2+}/Sr^{2+}$ exchange affects so strongly the $S_2$ multiline signal (*46*) whereas the substitution of a glutamine for D1-Glu189 which, from the 3D structures (*1*−*3*) is a bidantate ligand between the $Ca^{2+}$ and one Mn ion, has no effect.

In *Synechocystis* 6803, the D1-His332 mutants were also studied by thermolumiscence experiments. These measurements were done in whole cells (*69*). As in purified PSII, the centers were found to be inhibited after $S_2Tyr_Z^{\bullet}$ formation in the large majority of PSII centers, and the results were interpreted by a down shift of the Em of the $S_2/S_1$ couple in the D1-His332(Asp, Glu, Ser) mutants by 75, 50, and 7 mV, respectively (*69*). In *T. elongatus*, in agreement with the lack of EPR changes in the $S_2$ state, no change in the TL properties of the D1-His332 mutants was observed.

In *T. elongatus*, in contrast to $S_2$, differences have been detected here in the $S_3$ state in the D1-His332(Gln, Ser) mutants. The $S_3$ EPR signal is slightly modified and the $E_m$ of the $S_3/S_2$ couple is increased by ≤20 mV.

The similar field positions of the resonances in the $S_3$ signals in WT* PSII and the D1-His332 mutants strongly suggest that the zero field parameters are not significantly affected by the mutations. Nevertheless, reproducible differences were observed. Several possibilities can be put forward to explain such small differences; (i) the contribution of another signal which would suggest a possible heterogeneity in the $S_3$ state of the mutants. This would not be surprising since heterogeneities have been already observed in the $S_2$ multiline signal (*72*); (ii) small changes in Mn hyperfine interactions from the Mn nuclei which seem partially resolved in some spectra although with a low signal-to-noise ratio (see Supporting Information). So far we could not find conditions in which the $S_3$ EPR signal was detectable by 9 GHz pulse EPR. This likely originates from too fast relaxation times due to the high spin value, $S = 3$. This also precludes the detection of possible couplings between the nitrogens of D1-His332 and the $Mn_4Ca$ cluster. Further work will be required to solve all these questions.

Water binding is perturbed with both substrate binding sites in the $S_3$ state in the D1-His332Gln mutant. The tightly bound water at the slow exchange site is retained more tightly in the D1-His332Gln mutation with a ~3-fold slowing in exchange rate (Table 1). This retention could be expected to correlate with an increase in the formal charge of the metal binding site (*16*, *73*). The nature of the tightly bound substrate water is consistent with a metal site exhibiting unimolecular exchange based on a

correlation between the exchange rate and activation energy (*47*). Indeed, the tightly bound substrate water is also retained more weakly in $Sr^{2+}$ substituted PSII centers (*74*, Hillier and Boussac unpublished). The change in the rate in D1-His332Gln for the tightly bound substrate water molecule can be explained as an increased in charge associated with the $Mn_4Ca$ complex. The obvious explanation from this is a change in the ligand coordination sphere.

Alternatively, the D1-His332 could be a supporting ligand to a substrate water binding metal. However, it is unlikely that mutation of D1-His332 if serving as a ligand to the $Mn_4Ca$ complex goes uncompensated. That is to say that the mutation will not likely result in an open empty coordination site. Either a water molecule will instead bind, or the -C=O or $-NH_2$ donors that are present in the Gln side chain will act as donors.

The exchange rate of the faster exchangeable water increased in the D1-His332Gln mutant which is indicative of a weaker substrate binding site. The effect of the mutation on the two water exchange rates differs therefore in amplitude and in direction which indicates a dissimilar perturbation. We know less about the origin of the fast exchanging substrate water, but recent unpublished results do suggest an association with a metal site coordinated by CP43-Glu354 (Hillier, unpublished).

Ultimately, it is attractive to postulate that the D1-His332 is a direct ligand to a water substrate binding metal in $S_3$, but there remains the possibility for perturbations in the second coordination sphere that may manifest in changes regarding substrate exchange.

All the results above suggest that the D1-His332 is more involved in $S_3$ than in $S_2$. This could be one element of the conformational changes put forward in the $S_2$ to $S_3$ transition from the S-state dependence of Ca-depletion (*63*), EXAFS spectroscopy (*64*), differences of activation energy in $S_2$ and $S_3$ (*60*, *61*), and different reactivity's to exogenous reductants (*62*).

## ACKNOWLEDGMENT

Yu Matsuda and Thanh-Lan Lai are acknowledged for technical help. We would like to thank Takumi Noguchi and Hiroyuki Suzuki for setting up Thermoluminescence machine and helpful discussions and also Bill Rutherford for helpful discussions.

## SUPPORTING INFORMATION AVAILABLE

Fitting of the flash induced absorption changes at 292 nm and EPR spectra with an expended magnetic field scale. This material is available free of charge via the Internet at http://pubs.acs.org.

## REFERENCES

1. Ferreira, K. N., Iverson, T. M., Maghlaoui, K., Barber, J., and Iwata, S. (2004) Architecture of the photosynthetic oxygen-evolving center. *Science 303*, 1831–1838.
2. Loll, B., Kern, J., Saenger, W., Zouni, A., and Biesiadka, J. (2005) Towards complete cofactor arrangement in the 3.0 angstrom resolution structure of photosystem II. *Nature 438*, 1040–1044.
3. Guskov, A., Kern, J., Gabdulkhakov, A., Broser, M., Zouni, A., and Saenger, W. (2009) Cyanobacterial photosystem II at 2.9-angstrom resolution and the role of quinones, lipids, channels and chloride. *Nat. Struct. Mol. Biol. 16*, 334–342.
4. Murray, J. W., Maghlaoui, K., Kargul, J., Ishida, N., Lai, T.-L., Rutherford, A. W., Sugiura, M., Boussac, A., and Barber, J. (2008) X-ray crystallography identifies two chloride binding sites in the oxygen evolving centre of Photosystem II. *Energy Environ. Sci. 1*, 161–166.
5. Kawakami, K., Umena, Y., Kamiya, N., and Shen, J.-R. (2009) Location of chloride and its possible functions in oxygen evolving Photosystem II revealed by X-ray crystallography. *Proc. Natl. Acad. Sci. U. S. A. 106*, 8567–8572.
6. Diner, B. A., Schlodder, E., Nixon, P. J., Coleman, W. J., Rappaport, F., Lavergne, J., Vermaas, W. F., and Chisholm, D. A. (2001) Site-directed mutations at D1-His198 and D2-His97 of photosystem II in synechocystis PCC 6803: Sites of primary charge separation and cation and triplet stabilization. *Biochemistry 40*, 9265–9281.
7. Groot, M. L., Pawlowicz, N. P., van Wilderen, L. J., Breton, J., van Stokkum, I. H., and van Grondelle, R. (2005) Initial electron donor and acceptor in isolated Photosystem II reaction centers identified with femtosecond mid-IR spectroscopy. *Proc. Natl. Acad. Sci. U. S. A. 102*, 13087–13092.
8. Holzwarth, A. R., Muller, M. G., Reus, M., Nowaczyk, M., Sander, J., and Rögner, M. (2006) Kinetics and mechanism of electron transfer in intact photosystem II and in the isolated reaction center: Pheophytin is the primary electron acceptor. *Proc. Natl. Acad. Sci. U. S. A. 103*, 6895–6900.
9. Rappaport, F., and Diner, B. A. (2007) Primary photochemistry and energetics leading to the oxidation of the $(Mn)_4Ca$ cluster and to the evolution of molecular oxygen in Photosystem II. *Coord. Chem. Rev. 252*, 259–272.
10. Renger, G. (2007) Photosystem II: Structure and mechanism of the water-plastoquinone oxidoreductase. *Photosynth. Res. 92*, 407–425.
11. Kok, B., Forbush, B., and McGloin, M. P. (1970) Cooperation of charges in photosynthetic $O_2$ evolution. 1. A linear 4-step mechanism. *Photochem. Photobiol. 11*, 457–475.
12. Yano, J., Kern, J., Sauer, K., Latimer, M. J., Pushkar, Y., Biesiadka, J., Loll, B., Saenger, W., Messinger, J., Zouni, A., and Yachandra, V. K. (2006) Where water is oxidized to dioxygen: Structure of the photosynthetic $Mn_4Ca$ cluster. *Science 314*, 821–825.
13. McEvoy, J. P., and Brudvig, G. W. (2006) Water-splitting chemistry of photosystem II. *Chem. Rev. 106*, 4455–4483.
14. Rutherford, A. W., and Boussac, A. (2004) Water photolysis in biology. *Science 303*, 1782–1784.
15. Debus, R. J. (2007) Protein ligation of the photosynthetic oxygen-evolving center. *Coord. Chem. Rev. 252*, 244–258.
16. Hillier, W., and Wydrzynski, T. (2006) O18-Water exchange in photosystem II: Substrate binding and intermediates of the water splitting cycle. *Coord. Chem. Rev. 252*, 306–317.
17. Lubitz, W., Reijerse, E. J., and Messinger, J. (2008) Solar water-splitting into $H_2$ and $O_2$: design principles of photosystem II and hydrogenases. *Energy Environ. Sci. 1*, 15–31.
18. Betley, T. A., Surendranath, Y., Childress, M. V., Alliger, G. E., Fu, R., Cummins, C. C., and Nocera, D. G. (2008) A ligand field chemistry of oxygen generation by the oxygen-evolving complex and synthetic active sites. *Phil. Trans. R. Soc. B 263*, 1293–1303.
19. Sproviero, E. M., Shinopoulos, K., Gascón, J. A., McEvoy, J. P., Brudvig, G. W., and Batista, V. S. (2008) QM/MM computational studies of substrate water binding to the oxygen-evolving centre of photosystem II. *Phil. Trans. R. Soc. B 363*, 1149–1156.
20. Yano, J., Kern, J., Irrgang, K. D., Latimer, M. J., Bergmann, U., Glatzel, P., Pushkar, Y., Biesiad-ka, J., Loll, B., Sauer, K., Messinger, J., Zouni, A., and Yachandra, V. K. (2005) X-ray damage to the $Mn_4Ca$ complex in single crystals of photosystem II: A case study for metalloprotein crystallography. *Proc. Natl. Acad. Sci. U.S.A. 102*, 12047–12052.
21. Grabolle, M., Haumann, M., Muller, C., Liebisch, P., and Dau, H. (2006) Rapid loss of structural motifs in the manganese complex of oxygenic photosynthesis by X-ray irradiation at 10−300 K. *J. Biol. Chem. 281*, 4580–4588.
22. Clausen, J., and Junge, W. (2004) Detection of an intermediate of photosynthetic water oxidation. *Nature 430*, 480–483.
23. Haumann, M., Grundmeier, A., Zaharieva, I., and Dau, H. (2008) Photosynthetic water oxidation at elevated dioxygen partial pressure monitored by time-resolved X-ray absorption measurements. *Proc. Natl. Acad. Sci. U.S.A. 105*, 17384–17389.
24. Kimura, Y., Mizusawa, N., Yamanari, T., Ishii, A., and Ono, T.-A. (2005) Structural changes of D1 C-terminal alpha-carboxylate during S-state cycling in photosynthetic oxygen evolution. *J. Biol. Chem. 280*, 2078–2083.
25. Strickler, M. A., Hillier, W., and Debus, R. J. (2006) No evidence from FTIR difference spectroscopy that glutamate-189 of the D1 polypeptide ligates a Mn ion that undergoes oxidation during the S0 to S1, S1 to S2, or S2 to S3 transitions in photosystem II. *Biochemistry 45*, 8801–8811.
26. Kimura, Y., Mizusawa, N., Ishii, A., Nakazawa, S., and Ono, T.-A. (2005) Changes in structural and functional properties of

oxygen-evolving complex induced by replacement of D1-glutamate 189 with glutamine in photosystem II: Ligation of glutamate 189 carboxylate to the manganese cluster. *J. Biol. Chem. 280*, 37895–37900.
27. Strickler, M. A., Walker, L. M., Hillier, W., Britt, R. D., and Debus, R. J. (2007) No evidence from FTIR difference spectroscopy that aspartate-342 of the D1 polypeptide ligates a Mn ion that undergoes oxidation during the S0 to S1, S1 to S2, or S2 to S3 transitions in photosystem II. *Biochemistry 46*, 3151–3160.
28. Debus, R. J., Strickler, M. A., Walker, L. M., and Hillier, W. (2005) No evidence from FTIR difference spectroscopy that aspartate-170 of the D1 polypeptide ligates a manganese ion that undergoes oxidation during the S0 to S1, S1 to S2, or S2 to S3 transitions in photosystem II. *Biochemistry 44*, 1367–1374.
29. Strickler, M. A., Hwang, H. J., Burnap, R. L., Yano, J., Walker, L. M., Service, R. J., Britt, R, D., Hillier, W., and Debus, R. J. (2008) Glutamate-354 of the CP43 polypeptide interacts with the oxygen-evolving $Mn_4Ca$ cluster of photosystem II: a preliminary characterization of the Glu354Gln mutant. *Phil. Trans. R. Soc. B 363*, 1179–1187.
30. Debus, R. J., Campbell, K. A., Peloquin, J. M., Pham, D. P, and Britt, R. D. (2000) Histidine 332 of the D1 polypeptide modulates the magnetic and redox properties of the manganese cluster and tyrosine Y-Z in photosystem II. *Biochemistry 39*, 470–478.
31. Debus, R. J., Campbell, K. A., Gregor, W., Li, Z. L., Burnap, R. L., and Britt, R. D. (2001) Does histidine 332 of the D1 polypeptide ligate the manganese cluster in photosystem II? An electron spin echo envelope modulation study. *Biochemistry 40*, 3690–3699.
32. Hwang, H. J., Dilbeck, P., Debus, R. J., and Burnap, R. L. (2007) Mutation of arginine 357 of the CP43 protein of photosystem II severely impairs the catalytic S-state cycle of the $H_2O$ oxidation complex. *Biochemistry 46*, 11987–11997.
33. Hundelt, M., Hays, A. M. A., Debus, R. J., and Junge, W. (1998) Oxygenic photosystem II: The mutation D1-D61N in *Synechocystis* sp. PCC 6803 retards S-state transitions without affecting electron transfer from Y-Z to P-680(+). *Biochemistry 37*, 14450–14456.
34. Clausen, J., Debus, R. J., and Junge, W. (2004) Time-resolved oxygen production by PSII: chasing chemical intermediates. *Biochim. Biophys. Acta 1655*, 184–194.
35. Chu, H.-A., Nguyen, A. P., and Debus, R. J. (1995) Amino acid residues that influence the binding of manganese or calcium to Photosystem II. 2. The carboxy-terminal domain of the Dl polypeptide. *Biochemistry 34*, 5859–5882.
36. Sugiura, M., Boussac, A., Noguchi, T., and Rappaport, F. (2008) Influence of histidine-198 of the D1 subunit on the properties of the primary electron donor, P-680, of photosystem II in Thermosynechococcus elongatus. *Biochim. Biophys. Acta 1777*, 341–342.
37. Sugiura, M., Rappaport, F., Brettel, K., Noguchi, T., Rutherford, A. W., and Boussac, A. (2004) Site-directed mutagenesis of *Thermosynechococcus elongatus* photosystem II: the O-2 evolving enzyme lacking the redox active tyrosine D. *Biochemistry 43*, 13549–13563.
38. Sugiura, M., and Inoue, Y. (1999) Highly purified thermo-stable oxygen-evolving photosystem II core complex from the thermophilic cyanobacterium *Synechococcus elongatus* having his-tagged CP43. *Plant Cell Physiol. 40*, 1219–1241.
39. Boussac, A., Sugiura, M., Lai, T.-L., and Rutherford, A. W. (2008) Low temperature photochemistry in Photosystem II from *Thermosynechococcus elongatus* induced by visible and near-infrared light. *Phil. Trans. R. Soc. 363*, 1203–1210.
40. Boussac, A., Sugiura, M., Rutherford, A. W., and Dorlet, P. (2009) Complete EPR spectrum of the $S_3$-state of the oxygen-evolving Photosystem II. *J. Am. Chem. Soc. 131*, 5050–5051.
41. Ishida, N., Sugiura, M., Rappaport, F., Lai, T.-L., Rutherford, A. W., and Boussac, A. (2008) Biosynthetic exchange of bromide for chloride and strontium for calcium in the Photosystem II oxygen-evolving enzyme. *J. Biol. Chem. 283*, 13330–13340.
42. Béal, D., Rappaport, F., and Joliot, P. (1999) A new high-sensitivity 10-ns time-resolution spectrophotometric technique adapted to in vivo analysis of the photosynthetic apparatus. *Rev. Sci. Instrum. 70*, 202–207.
43. Noguchi, T., Katoh, M., and Inoue, Y. (2002) A new system for detection of thermoluminescence and delayed fluorescence from photosynthetic apparatus with precise temperature control. *Spectroscopy 16*, 89–94.
44. Styring, S., and Rutherford, A. W. (1987) In the oxygen-evolving complex of photosystem II the S0 state is oxidized to the S1 state by D+ (signal II slow). *Biochemistry 26*, 2401–2405.
45. Isgandarova, S., Renger, G., and Messinger, J. (2003) Functional differences of photosystem II from Synechococcus elongatus and spinach characterized by flash induced oxygen evolution patterns. *Biochemistry 42*, 8929–8938.
46. Boussac, A., Rappaport, F., Carrier, P., Verbavatz, J.-M., Gobin, R., Kirilovsky, D., Rutherford, A. W., and Sugiura, M. (2004) Biosynthetic $Ca^{2+}/Sr^{2+}$ exchange in the photosystem II oxygen evolving enzyme of *Thermosynechococcus elongatus*. *J. Biol. Chem. 279*, 22809–22819.
47. Messinger, J., Badger, M., and Wydrzynski, T. (1995) Detection of one slowly exchanging substrate water molecule in the S3-state of Photosystem-II. *Proc. Natl. Acad. Sci. U.S.A. 92*, 3209–3213.
48. Singh, S., Debus, R. J., Wydrzynski, T., and Hillier, W. (2008) Investigation of substrate water interactions at the high-affinity Mn site in the photosystem II oxygen-evolving complex. *Phil. Trans. R. Soc. B 363*, 1229–1234.
49. Hillier, W., and Wydrzynski, T. (2004) Substrate water interactions within the Photosystem II oxygen evolving complex. *Phys. Chem. Chem. Phys. 6*, 4882–4889.
50. Rappaport, F., Blanchard-Desce, M., and Lavergne, J. (1994) Kinetics of electron-transfer and electrochromic change during the redox transitions of the photosynthetic oxygen-evolving complex. *Biochim. Biophys. Acta 1184*, 178–192.
51. Lavergne, J. (1991) Improved UV-visible spectra of the s-transitions in the photosynthetic oxygen-evolving system. *Biochim. Biophys. Acta 1060*, 175–188.
52. Lavorel, J. (1978) Matrix analysis of the oxygen evolving system of photosynthesis. *J. Theor. Biol. 57*, 171–185.
53. Dismukes, G. C., and Siderer, Y. (1981) Intermediates of a polynuclear manganese center involved in photosynthetic oxidation of water. *Proc. Natl. Acad. Sci. U. S. A. 1978*, 274–278.
54. Peloquin, J. M., Campbell, K. A., Randall, D. W., Evanchik, M. A., Pecoraro, V. L., Armstrong, W. H., and Britt, R. D. (2000) Mn55 ENDOR of the S2-state multiline EPR signal of photosystem II: Implications on the structure of the tetranuclear Mn cluster. *J. Am. Chem. Soc. 122*, 10926–10942.
55. Charlot, M.-F., Boussac, A., and Blondin, G. (2005) Towards a spin coupling model for the $Mn_4$ cluster in Photosystem II. *Biochim. Biophys. Acta 1708*, 120–132.
56. Kulik, L. V., Epel, B., Lubitz, W., and Messinger, J. (2007) Electronic structure of the $Mn_4OxCa$ cluster in the S-0 and S-2 states of the oxygen-evolving complex of photosystem II based on pulse Mn-55-ENDOR and EPR Spectroscopy. *J. Am. Chem. Soc. 129*, 13421–13435.
57. Boussac, A., Sugiura, M., Inoue, Y., and Rutherford, A. W. (2000) EPR study of the oxygen evolving complex in His-tagged photosystem II from the cyanobacterium. *Synechococcus elongatus*. *Biochemistry 39*, 13788–13799.
58. Kerfeld, C. A., Sawaya, M. R., Bottin, H., Tran, K. T., Sugiura, M., Cascio, D., Desbois, A., Yeates, T. O., Kirilovsky, D., and Boussac, A. (2003) Structural and EPR Characterization of the soluble form of Cytochrome c-550 and of the *psbV2* gene product from the cyanobacterium. *Thermosynechococcus elongatus. Plant Cell Physiol. 44*, 697–706.
59. Boussac, A., Deligiannakis, Y., Rutherford, A. W. (1998) Effects of methanol on the $Mn_4$-cluster of Photosystem II. .Photosynthesis: Mechanisms and effects (Garab, G., Ed.) Vol II, pp 1233−1240, Kluwer Academic Publisher.
60. Koike, H., Hanssum, B., Inoue, Y., and Renger, G. (1987) Temperature-dependence of S-state transition in a thermophilic cyanobacterium, *Synechococcus vulcanus* copeland measured by absorption changes in the ultraviolet region. *Biochim. Biophys. Acta 893*, 524–533.
61. Renger, G, and Hanssum, B. (1992) Studies on the reaction coordinates of the water oxidase in PSII membrane-fragments from Spinach. *FEBS Lett. 299*, 28–32.
62. Messinger, J., Wacker, U., and Renger, G. (1991) Unusual low reactivity of the water oxidase in redox state S3 toward exogenous reductants - analysis of the $NH_2OH$-induced and NH2NH2-induced modifications of flash-induced oxygen evolution in isolated spinach thylakoids. *Biochemistry 30*, 7852–7862.
63. Boussac, A., and Rutherford, A. W. (1988) $Ca^{2+}$ binding to the oxygen evolving enzyme varies with the redox state of the Mn cluster. *FEBS Lett. 236*, 432–436.
64. Pushkar, Y., Yano, J., Sauer, K., Boussac, A., and Yachandra, V. (2008) Structural Changes in the $Mn_4Ca$ Cluster and the Mechanism of Photosynthetic Water Splitting. *Proc. Natl. Acad. Sci. U. S. A. 105*, 1879–1884.
65. Fufezan, C., Gross, C. M., Sjödin, M., Rutherford, A. W., Krieger-Liszkay, A., and Kirilovsky, D. (2007) Influence of the redox potential of the primary quinone electron acceptor on photoinhibition in photosystem II. *J. Biol. Chem. 282*, 12492–12502.

66. Rappaport, F., and Lavergne, J. (2009) Thermoluminescence: Theory. *Photosynth. Res.* in press.
67. Cser, K., and Vass, I. (2007) Radiative and non-radiative charge recombination pathways in Photosystem II studied by thermoluminescence and chlorophyll fluorescence in the cyanobacterium Synechocystis 6803. *Biochim. Biophys. Acta 1767*, 233–243.
68. Rappaport, F., Cuni, A., Xiong, L., Sayre, R., and Lavergne, J. (2005) Charge recombination and thermoluminescence in Photosystem II. *Biophys. J. 88*, 1948–1958.
69. Allahverdiyeva, Y., Deak, Z., Szilard, A., Diner, B. A., Nixon, P. J., and Vass, I. (2004) The function of D1-H332 in Photosystem II electron transport studied by thermoluminescence and chlorophyll fluorescence in site-directed mutants of Synechocystis 6803. *Eur. J. Biochem. 271*, 3523–3532.
70. Tang, X. S., Diner, B. A., Larsen, B. S., Gilchrist, M. L., Lorigan, G. A., and Britt, R. D. (1994) Identification of histidine at the catalytic site of the photosynthetic oxygen-evolving complex. *Proc. Natl. Acad. Sci. U. S. A. 91*, 704–708.
71. Strickler, M. A., Walker, L. M., Hillier, W., and Debus, R. J. (2005) Evidence from biosynthetically incorporated strontium and FTIR difference spectroscopy that the C-terminus of the D1 polypeptide of Photosystem II does not ligate calcium. *Biochemistry 44*, 8571–8577.
72. Boussac, A. (1997) Inhomogeneity of the EPR multiline signal from the S2-state of the photosystem II oxygen evolving enzyme. *J. Biol. Inorg. Chem. 2*, 580–585.
73. Hillier, W., and Wydrzynski, T. (2001) Oxygen ligand exchange at metal sites - implications for the $O_2$ evolving mechanism of Photosystem II. *Biochim. Biophys. Acta 1503*, 197–209.
74. Hendry, G., and Wydrzynski, T. (2003) O-18 isotope exchange measurements reveal that calcium is involved in the binding of one substrate-water molecule to the oxygen-evolving complex in Photosystem II. *Biochemistry 42*, 6209–6217.